Available online at www.sciencedirect.com
ScienceDirect
Electric Power Systems Research 78 (2008) 849–860
ELECTRIC POWER SYSTEMS RESEARCH
www.elsevier.com/locate/epsr

Impact of saturation nonlinearities/disturbances on the small-signal stability of power systems: An analytical approach

H. Xin [a,*], D. Gan [a,1], Z. Qu [b], J. Qiu [a]

[a] College of Electrical Engineering, Zhejiang University, Hangzhou, Zhejiang, China
[b] School of EECS, University of Central Florida, 4000 Central Florida Blvd., Orlando, FL 32816-2450, USA

Received 30 January 2007; received in revised form 6 June 2007; accepted 8 June 2007
Available online 6 August 2007

Abstract

In this paper, a multi-objective optimization model is presented to estimate the practical stability region and maximum endurable disturbance rejection for a small-signal power system dynamic model with saturation nonlinearities and disturbance rejection. Iterative algorithms are developed to solve for Pareto optimized solutions (POS) of this optimization. Furthermore, as an application of this approach to power systems, a method to analyze the impact of saturation nonlinearities and disturbance rejection on power system small-signal stability is introduced based on the estimated stability region and maximum endurable disturbance rejection. Numerical results of a test power system with detailed saturated PSS controllers are described, indicating the reliability and simplicity of the method.

Keywords: Saturated systems; Power system stabilizer (PSS); Multi-objective optimization; Practical stability region; Golden section search (GSS) method; Iterative algorithm

1. Introduction

To improve the small-signal stability of power systems, much has relied on power system stabilizers (PSS) [1]. Thus, the issues of PSS parameter optimization [2,3] and control law design [4,5] are of interest. However, more often than not, the saturation nonlinearities, either intentionally designed or resulting from the limitations of equipments, are ubiquitous in the engineering fields [6], such as the power systems [7,8]. In general, PSS controllers are also subject to the saturation nonlinearities and disturbance rejection, which unavoidably affect the performance of PSS [9] and even can lead to loss of stability [6].

Therefore, if the saturation exists, the performance of the PSS control systems designed without considering saturation nonlinearities and disturbance rejection may seriously deteriorate [9]. Furthermore, the disturbance rejection may lead to the inexistence of stability region [10,11]. Utility engineers did look at the issue, mainly relying on extensive simulation studies [7,8]. Little attention has been paid to investigate the impact of such factors on system stability from analytical perspective.

The aim of this paper is to provide analytical methods to analyze the impact of saturation nonlinearities on power system small-signal stability when disturbance rejection exists, based on our recent work [9], where saturation nonlinearities are considered but the disturbance rejection is ignored. PSS performance study is taken as an example. The key is to characterize the stability region and maximum endurable disturbance rejection.

However, it is very difficult to handle the above-mentioned task today [6,10], since saturation nonlinearities make a simple linear system become a complex nonlinear system [10–12]. Therefore, many researches focus on the study of estimating stability region in recent years, e.g. [6,12] and the references therein, in which Hu derives a promising method to obtain an ellipsoid inside stability region by a quadratic Lyapunov function based on a convex LMI optimization [6]. This idea has been used in our recent work [9], and good results are obtained. Nevertheless, the disturbance rejection issue is not considered. In order to conquer this limitation, in some references, say [6,13], an invariant ellipse is derived as the practical stability region estimation, but an efficient algorithm is still lacking. In fact, in

* Corresponding author. Tel.: +86 571 87951831; fax: +86 571 87952591.
E-mail addresses: eexinhh@gmail.com (H. Xin), deqiang.gan@ieee.org (D. Gan), qu@mail.ucf.edu (Z. Qu).
[1] +86 571 87951831.

0378-7796/$ – see front matter © 2007 Elsevier B.V. All rights reserved.
doi:10.1016/j.epsr.2007.06.006

these papers, an auxiliary parameter is searched by a grid search mechanism, and the maximum endurable disturbance rejection is obtained by enumeration, so it unavoidably requires extensive computation burden.

To overcome this problem, we propose a multi-objective optimization model [14] to estimate the practical stability region and the maximum endurable disturbance rejection on the basis of [6,13]. Iterative algorithms are provided to solve for Pareto optimized solutions (POS) of this optimization, and some properties of these algorithms are proved also. Moreover, the procedures of the iterative algorithms are very simple and can be handled efficiently by the toolbox in Matlab.

The structure of the paper is as follows. In Section 2, the model of power systems with saturation nonlinearities and disturbance rejection is presented. Section 3 provides a multi-objective optimization model for estimating the practical stability region and maximum endurable disturbance rejection. The algorithms for solving for POS of the multi-object optimization problem are developed in Section 4. Based on the POS, a method to analyze the performance of PSS in power systems is provided in Section 5. In Section 6, a numerical example is described, indicating the reliability and simplicity of this approach. Section 7 draws the main conclusions of this work.

2. Power system model with saturation nonlinearities and disturbance rejection

Within a neighborhood around a given operating point, the ideal linear state space model of a power system can be expressed as [1,11]:

$$\dot{\boldsymbol{x}}(t) = \boldsymbol{A}'\boldsymbol{x}(t) + \boldsymbol{B}\boldsymbol{u}(t) + \boldsymbol{E}\boldsymbol{w}(t); \quad \boldsymbol{x}_0 \in X_0, \boldsymbol{w}(t) \in W \tag{1}$$

where $\boldsymbol{x} \in R^n$ is the state; $\boldsymbol{u} \in R^m$ is the control; $\boldsymbol{A}' \in R^{n\times n}$ is the system matrix; $\boldsymbol{x}_0$ denotes the initial states; X_0 is the set of all initial states under consideration, $\boldsymbol{w}(t)$ denotes the disturbance rejection; $W \subset R^l$ is the set of all disturbance rejection under consideration and matrix $\boldsymbol{E}$ is the corresponding disturbance rejection matrix, respectively.

Due to actuator saturation which is considered to be a anti-windup function in this paper, a more realistic model is [6]:

$$\dot{\boldsymbol{x}} = \boldsymbol{A}'\boldsymbol{x} + \boldsymbol{B}sat(\boldsymbol{u}) + \boldsymbol{E}\boldsymbol{w} \tag{2}$$

where sat(·) is a saturation function which is symmetric with respect to the origin, i.e.:

$$\mathrm{sat}(\boldsymbol{u}) = [\mathrm{sat}_1(u_1), \mathrm{sat}_2(u_2), \ldots, \mathrm{sat}_m(u_m)]^{\mathrm{T}},$$

$$\mathrm{sat}_i(u_i) = \begin{cases} \bar{u}_i | u_i | > \bar{u}_i \\ u_i | u_i | \le \bar{u}_i \end{cases} \tag{3}$$

Thus, under a linear feedback control of form $\boldsymbol{u} = \boldsymbol{G}\boldsymbol{x}$, the closed loop system becomes

$$\dot{\boldsymbol{x}} = \boldsymbol{A}'\boldsymbol{x} + \boldsymbol{B}\mathrm{sat}(\boldsymbol{G}\boldsymbol{x}) + \boldsymbol{E}\boldsymbol{w} \tag{4}$$

where pair $\{\boldsymbol{A}', \boldsymbol{B}\}$ is assumed to be controllable [11], $\boldsymbol{G} \in R^{m\times n}$ is the feedback gain matrix such that $Re(\lambda_i) < 0$ for all eigenvalues λ_i of matrix $\boldsymbol{A}' + \boldsymbol{B}\boldsymbol{G}$, and $Re(\lambda_i)$ denotes the real part of λ_i.

In our recent work [9], we did not consider the impact of disturbance rejection $\boldsymbol{w}(t)$ on the dynamic behaviors of the saturated system. In system (4), should disturbance rejection $\boldsymbol{w}$ be persistent, the origin is no longer an equilibrium point nor is it Lyapunov stable [10]. In this case, robust stability concepts such as uniform ultimate boundedness [10,15], also referred to as practical stability [11,16], can be applied to system (4). In particular, system (4) is said to be uniformly ultimately bounded (UUB) with respect to X_0 and W if, for all $\boldsymbol{x}_0 \in X_0$ and for every $\boldsymbol{w} \in W$, solution $\boldsymbol{x}(t)$ to Eq. (9) converges to a specified neighborhood around the origin. As such, the following region of practical stability is introduced for the subsequent investigation of system (4):

$$\Omega = \{\boldsymbol{x}_0 \in X_0 | \varphi_t(\boldsymbol{x}_0, \boldsymbol{w}) \text{ is UUB for every choice of } \boldsymbol{w} \in \boldsymbol{W}\} \tag{5}$$

where $\varphi_t(\boldsymbol{x}_0, \boldsymbol{w})$ denotes the trajectory of system (4) starting from the initial state $\boldsymbol{x}_0$. For simplicity, we make no difference between the terms "practical stability region" and "stability region" later.

From the definition of the stability region, the saturation nonlinearities result in that only the states in Ω can be considered to be stable. Furthermore, in order to analyze the impact of disturbance rejection on the dynamic behaviors of (4), we introduce a parameter, say α, for measuring the magnitude of disturbance rejection, i.e., we suppose that the disturbance rejection set W can be expressed as

$$W = \{\boldsymbol{w} \in R^l | \boldsymbol{w}^{\mathrm{T}}\boldsymbol{w} \le \alpha\} \tag{6}$$

Clearly, the relationship between W and α is

$$\alpha = \max_{\boldsymbol{w}\in W} \{\boldsymbol{w}^{\mathrm{T}}\boldsymbol{w}\} \tag{7}$$

To analyze the dynamic performance of system (4) later, we further consider set X_0 of expected initial states is a high-dimension ellipse defined as

$$X_0 = \{\boldsymbol{x} \in R^n | \boldsymbol{x}^{\mathrm{T}}\boldsymbol{P}_0\boldsymbol{x} \le \beta^2\} \tag{8}$$

where $\beta > 0$ is a variable to be decided later and $P_0 \in R^{n\times n}$ is a given and nonnegative definite symmetric matrix which is considered to be an identify matrix in the simulation. Namely, we assume that the expected initial states can be contained by an ellipse with fixed shape and variable size.

So from the previous analysis, the closed loop and asymptotically stable linear model:

$$\dot{\boldsymbol{x}} = (\boldsymbol{A}' + \boldsymbol{B}\boldsymbol{G})\boldsymbol{x} + \boldsymbol{E}\boldsymbol{w} := \boldsymbol{A}\boldsymbol{x} + \boldsymbol{E}\boldsymbol{w} \tag{9}$$

is valid only for the states inside the polyhedron F, defined in the state space as

$$F = \{\boldsymbol{x} \in R^n | -\bar{\boldsymbol{u}} \le \boldsymbol{G}\boldsymbol{x} \le \bar{\boldsymbol{u}}\} \tag{10}$$

where the inequalities are based on "elements by elements", i.e., $F = \{\boldsymbol{x} | -\bar{u}_i \le \boldsymbol{g}_i\boldsymbol{x} \le \bar{u}_i, i = 1, 2, \ldots, m\}$ and g_i is the ith line of feedback gain matrix $\boldsymbol{G}$.

Outside set F in which a power system of form (4) behaves as a linear system, however, the dynamic behaviors of system (4) are difficult to analyze directly. Thus, a power system of form (4) is not globally UUB usually. Clearly, practical stability region Ω depends upon property of matrix pair $\{\boldsymbol{A}',\boldsymbol{B}\}$, saturation threshold $\bar{\boldsymbol{u}}$, and disturbance rejection set W. In particular, once magnitude of the disturbance rejection is allowed to exceed certain value, the maximum endurable value and denoted by $\alpha_{\max}$, the saturated control can no longer compensate for its destabilizing effort. Therefore, both the stability region and the maximum endurable disturbance rejection should be determined for power system applications and, since they are mutually dependent, their solutions can be found through a multiple-objective optimization to be formulated in the next section.

3. Estimation of stability region and maximum disturbance rejection set

In this section, an algorithm is proposed to estimate both stability region Ω and maximum endurable disturbance rejection set W under the following assumption.

Assumption 1. In system (4), matrix $\boldsymbol{A}=\boldsymbol{A}'+\boldsymbol{BG}$ is a Hurwitz matrix, i.e., all the eigenvalues of $\boldsymbol{A}$ satisfy $Re(\lambda_i)<0$; set W is uniformly bounded, and the threshold values $\bar{u}_i > 0$ for all $i=1, 2, \ldots, m$.

Remark 1. Matrix $\boldsymbol{A}$ being Hurwitz can always be ensured if pair $\{\boldsymbol{A}',\boldsymbol{B}\}$ is controllable. If any of the threshold values $\bar{u}_i$ is zero, there will be no control through the corresponding channel, and equivalently matrix $\boldsymbol{B}$ is degenerate. It is obvious that Assumption 1 is necessary for stabilization of system (1) and its robustness against disturbance rejection.

For system (2), if the expected initial states and expected disturbance rejection can be stabilized by control $\boldsymbol{u}=\boldsymbol{Gx}$, then the control is called to be effective [11]. Clearly, the analysis of the impact of saturation nonlinearities on the stability of system (4) is equal to the analysis of the saturated control performance, thus we will provide a method in Section 5 for analyze the effectiveness of saturated controls by the analysis of the system stability.

Assumption 1 implies that the trajectory $\varphi_t(\boldsymbol{x}_0, \boldsymbol{w})$ of system (4) is UUB globally if we ignore the saturation nonlinearities, and control $\boldsymbol{u}=\boldsymbol{Gx}$ is effective consequently. However, the input saturations in general reduce the stability region to a bounded set, and only the initial states in the stability region can be stabilized from the definition of the stability region in expression (5). Therefore, to analyze the effectiveness of the saturated control or to analyze the impact of the saturation nonlinearities on the performance of system (4), one only needs to calculate the stability region and the corresponding disturbance rejection set W of system (4). Unfortunately, it is very difficult to handle the work mentioned above since system (4) becomes nonlinear due to saturation function sat(·). In this paper, Ω and W are estimated by the Lyapunov direct method.

3.1. Theoretical results for stability region and disturbance rejection set

To introduce the theories for estimating the stability (Ω) and the maximum endurable value of W, we first introduce the following two lemmas.

Lemma 1. *Consider system (4). If its trajectory remains within F for all $t\geq 0$ and for all initial states in set $\tilde{\Omega}$, that is, $\varphi_t(\boldsymbol{x}_0, \boldsymbol{w})\in F$ for all $(t, x_0)\in[0, +\infty)\times\tilde{\Omega}$ and all $\boldsymbol{w}\in W$, then set $\tilde{\Omega}$ is a subset of stability region Ω for system (4).*

Proof. Since $\varphi_t(\boldsymbol{x}_0, w)$ remains within F for any $x_0\in\tilde{\Omega}$, system (4) operates without the saturation nonlinearity. By Assumption 1, the corresponding linear system matrix is Hurtiwz, thus from [11] its trajectory is UUB with respect to disturbance rejection set W, i.e., $\varphi_t(\boldsymbol{x}_0, w)\in\Omega$. In other words, if $\boldsymbol{x}_0\in\tilde{\Omega}$, then $\boldsymbol{x}_0\in\Omega$. In short, $\tilde{\Omega}\subset\Omega$ is proved. □

Lemma 2. [6]. *Let Ω_0 be the set defined by*

$$\Omega_0=\{\boldsymbol{x}\in R^n \mid V(\boldsymbol{x})=\boldsymbol{x}^{\mathrm{T}}\boldsymbol{P}\boldsymbol{x}\leq c\} \tag{11}$$

where P is a given positive definite matrix, $c=\min_{\boldsymbol{x}\in\partial F}(V(\boldsymbol{x}))$ and ∂F represents the boundary of F.

Then, $\Omega_0\subset F$.

The following theorem can be stated based on Lemmas 1 and 2.

Theorem 1. *Consider system (4) in which the disturbance rejection set W is defined as in (6). If there exist a positive constant η and a positive definite symmetric matrix $\boldsymbol{P}\in R^{n\times n}$, such that*

$$\boldsymbol{A}^{\mathrm{T}}\boldsymbol{P}+\boldsymbol{P}\boldsymbol{A}+\frac{1}{\eta}\boldsymbol{P}\boldsymbol{E}\boldsymbol{E}^{\mathrm{T}}\boldsymbol{P}+\frac{\eta\alpha}{c}\boldsymbol{P}<0 \tag{12}$$

is satisfied, then $\Omega_0\subset\Omega$ holds. Here, $\boldsymbol{A}=\boldsymbol{A}'+\boldsymbol{BG}$; c, $V(x)$ and Ω_0 are defined in (11); α is the disturbance rejection magnitude defined in (7).

Proof. The time derivative of $V(\boldsymbol{x})=\boldsymbol{x}^{\mathrm{T}}\boldsymbol{P}\boldsymbol{x}$ along system (9) is

$$\dot{V}(x)=\boldsymbol{x}^{\mathrm{T}}(\boldsymbol{A}^{\mathrm{T}}\boldsymbol{P}+\boldsymbol{P}\boldsymbol{A})\boldsymbol{x}+2\boldsymbol{x}^{\mathrm{T}}\boldsymbol{P}\boldsymbol{E}\boldsymbol{w} \tag{13}$$

Since $2ab\leq\eta a^{\mathrm{T}}a+\eta^{-1}b^{\mathrm{T}}b$ is satisfied for all $a,b\in R^n$ and $\eta>0$, $2\boldsymbol{x}^{\mathrm{T}}\boldsymbol{P}\boldsymbol{E}\boldsymbol{w}\leq\eta^{-1}\boldsymbol{x}^{\mathrm{T}}\boldsymbol{P}\boldsymbol{E}\boldsymbol{E}^{\mathrm{T}}\boldsymbol{P}\boldsymbol{x}+\eta\boldsymbol{w}^{\mathrm{T}}\boldsymbol{w}$ holds. Thus, from (12)–(13) and the definition of α in (7), it follows that

$$\begin{aligned}\dot{V}(x)&<\boldsymbol{x}^{\mathrm{T}}(\boldsymbol{A}^{\mathrm{T}}\boldsymbol{P}+\boldsymbol{P}\boldsymbol{A}+\eta^{-1}\boldsymbol{P}\boldsymbol{E}\boldsymbol{E}^{\mathrm{T}}\boldsymbol{P})\boldsymbol{x}\\&\quad+\eta\boldsymbol{w}^{\mathrm{T}}\boldsymbol{w}\leq-\eta\alpha c^{-1}\boldsymbol{x}^{\mathrm{T}}\boldsymbol{P}\boldsymbol{x}+\eta\alpha\end{aligned} \tag{14}$$

is satisfied when $\boldsymbol{x}\neq 0$ [6]. Since $\boldsymbol{x}\in\Omega_0$ implies $V(\boldsymbol{x})=\boldsymbol{x}^{\mathrm{T}}\boldsymbol{P}\boldsymbol{x}\leq c$, from (14) it follows that

$$\dot{V}(x)<-\eta\alpha c^{-1}\boldsymbol{x}^{\mathrm{T}}\boldsymbol{P}\boldsymbol{x}+\eta\alpha\leq-\eta\alpha c^{-1}c+\eta\alpha=0 \tag{15}$$

is satisfied for all $\boldsymbol{x}\in\Omega_0-\{0\}$. Thus, from (15) Ω_0 is an invariant set of (9). By Lemma 2, $\Omega_0\subset F$ is satisfied, and system (4) degenerates into system (9) in set F, so Ω_0 is also an invariant set of system (4), i.e., $\varphi_t(\boldsymbol{x}, w)\in\Omega_0\subset F$ holds for all $\boldsymbol{x}\in\Omega_0$. By Lemma 1, the conclusion of $\Omega_0\subset\Omega$ is drawn. □

Obviously, once some variables, such as $\boldsymbol{P}$, α and η, etc., are derived, Ω_0 can be obtained directly from expression (11). Hence Theorem 1 provides a method to estimate the stability region of system (4) and the stability region is a subset of F. To further apply this method to power systems conveniently, we extend system (4) with polyhedron F to more general constrained system as follows:

$$\dot{\boldsymbol{x}} = \boldsymbol{A}\boldsymbol{x} + \boldsymbol{E}\boldsymbol{w}, \quad -\bar{\boldsymbol{u}} \le \boldsymbol{G}\boldsymbol{x} \le \bar{\boldsymbol{u}}, \quad \boldsymbol{w} \in W, \quad \boldsymbol{x}_0 \in X_0 \tag{16}$$

to which Theorem 1 can be applied. Although Ω_0 concluded in Theorem 1 is a conservative estimate of Ω, determination of Ω_0 is quite involved but can be done according to the following process:

- Step 1: Verify Assumption 1. If it holds, continue; otherwise, Ω_0 cannot be found.
- Step 2: Calculate set F according to (10).
- Step 3: Determine solutions $\boldsymbol{P}$, η and α to Riccati equation (12).
- Step 4: Calculate Ω_0, the estimate of stability region, according to (12).

As mentioned previously, to analyze the performance of a control or to analyze the impact of the saturation nonlinearities on the performance of a dynamic system, the key is to estimate the stability region and disturbance rejection set, and this can be done via the above process. However, the most critical step in the above process is to find solutions $\boldsymbol{P}$, η and α, and arbitrary choose of them will lead to extremely conservative results unavoidably. In particular, the larger the set X_0 which can be contained by Ω_0, the less conservative the results are; similarly, the larger the endurable disturbance rejection set W, the less conservative the results are. Hence, for applications, it would be very useful to obtain the maximum endurable disturbance rejection set W and X_0 which can be contained by the estimated stability region Ω_0 as large as possible (characterized by $\alpha_{\max}$ and $\beta_{\max}$, respectively). This leads to a multi-objective optimization problem to be formulated in the next subsection.

3.2. An optimization approach for stability region and disturbance rejection

The numerical process introduced in the last section needs to be made less conservative by finding the best (i.e., largest) values of β and α to ensure stability of the closed-loop system (16). Accordingly, from Theorem 1, the following multi-objective optimization problem is formulated:

$$\begin{cases} (\alpha^*, \beta^*) = \max\limits_{P>0,\eta>0} (\alpha, \beta) \\ \text{s.t.} \quad \text{(a)} \quad X_0 = \{\boldsymbol{x} \in R^n | x^{\mathrm{T}} P_0 x \le \beta^2\} \subset \Omega_0 = \{\boldsymbol{x} \in R^n | V(x) = x^{\mathrm{T}} P x \le c\} \\ \qquad\quad \text{(b)} \quad c = \min\limits_{x \in \partial F} (V(\boldsymbol{x})) \\ \qquad\quad \text{(c)} \quad \boldsymbol{A}^{\mathrm{T}}\boldsymbol{P} + \boldsymbol{P}\boldsymbol{A} + \eta^{-1}\boldsymbol{P}\boldsymbol{E}\boldsymbol{E}^{\mathrm{T}}\boldsymbol{P} + \eta\alpha c^{-1}\boldsymbol{P} \le 0 \end{cases} \tag{17}$$

where superscript "*" denotes the optimal value of the argument; constraint (a) means that the set X_0 of expected initial states is in the estimated stability region Ω_0, i.e., the trajectories of system (4) starting from Ω_0 is stable (UUB); constraint (b) means the condition that Theorem 1 requires, i.e., Ω_0 resides within set F; constraint (c) is another condition that Theorem 1 requires, i.e., expression (12) is satisfied.

Clearly, (17) is a multi-objective, multi-variable, nonlinear problem. A global optimal solution to such a problem may not exist, hence the so-called Pareto optimal solution (POS) is often sought instead [14]. We will first outline POS and their algorithms/properties in Section 4, while what heuristics and engineering application background/knowledge needed will be discussed in Section 5.

4. Algorithms for multi-objective optimization

The concept of Pareto, as described below, is standard.

Definition 1 *((Deb [14]))*. Consider the multi-object optimization problem as follows:

$$\max_{x \in X} \boldsymbol{f}(\boldsymbol{x}) = (f_1(\boldsymbol{x}), f_2(\boldsymbol{x}), \ldots, f_n(\boldsymbol{x})) \tag{18}$$

For two points, say $\boldsymbol{x}_1$ and $\boldsymbol{x}_2$, in feasible set $\boldsymbol{X}$, if $f_i(\boldsymbol{x}_1) \ge f_i(\boldsymbol{x}_2)$ holds for all $1 \le i \le n$, and the equalities do not hold simultaneously, then we call that $\boldsymbol{x}_2$ is worse than $\boldsymbol{x}_1$ (denoted by $\boldsymbol{f}(\boldsymbol{x}_1) > \boldsymbol{f}(\boldsymbol{x}_2)$). If $\boldsymbol{x}$ is not worse than any other points in $\boldsymbol{X}$, then $\boldsymbol{x}$ is termed as a Pareto optimal solution (POS) of (18).

From this definition, the property on the POS of problem (17) can be derived immediately.

Theorem 2. *β^* is decreasing strictly with respect to the increase of α^*, where (α^*,β^*) denotes the POR of problem (17).*

Proof. Arbitrarily choose two POS of (17), say (α_1,β_1) and (α_2,β_2), and suppose $\alpha_1 > \alpha_2$ without loss of generality. To prove the theorem, we only need to prove $\beta_1 < \beta_2$. We use a contradiction argument.

Suppose that $\beta_1 < \beta_2$ is not satisfied, i.e., $\beta_1 \ge \beta_2$, so $(\alpha_1,\beta_1) \ge (\alpha_2,\beta_2)$ is satisfied. But $\alpha_1 > \alpha_2$ implies the equalities do not hold simultaneously, thus, (α_2,β_2) is worse than (α_1,β_1) from Definition 1, i.e., (α_2,β_2) is not a POS of problem (17) from he Definition 1 of POS. It is a contradictory conclusion. □

This theorem shows that the elements of POS, β^* and α^*, are of inverse proportion. As discussed in the simulation section, this important property can help us choose a practical POS when the method is applied to power systems. Next, we will discuss how to obtain the POS of (17).

4.1. Transformation of the constraints

Constraints (a), (b) and (c) are nonlinear in optimization problem (17). The standard tool that can simplify such constraints is Schur complements. Namely, suppose that $\boldsymbol{Q} > 0$, then

$$\boldsymbol{R} - \boldsymbol{S}\boldsymbol{Q}^{-1}\boldsymbol{S}^{\mathrm{T}} \ge 0 \Leftrightarrow \begin{bmatrix} \boldsymbol{R} & \boldsymbol{S} \\ \boldsymbol{S}^{\mathrm{T}} & \boldsymbol{Q} \end{bmatrix} \ge 0 \tag{19}$$

where symbol "⇔" means if and only if.

Let

$$\gamma = \beta^{-2}, \qquad \boldsymbol{R} = c\boldsymbol{P}^{-1}, \qquad z_i = \boldsymbol{g}_i\boldsymbol{R}, \quad i = 1, 2, \ldots, m, \quad \eta_1 = c(\eta\alpha)^{-1} \tag{20}$$

By (19), we can derive the following transformation, which also can be found in [6,9].

Constraint (a) is equivalent to

$$X_0 \subset \Omega_0 \Leftrightarrow \beta^{-2}P_0 - c^{-1}\boldsymbol{P} \geq 0 \Leftrightarrow \gamma P_0 - R^{-1} \geq 0 \Leftrightarrow \begin{bmatrix} \gamma\boldsymbol{P}_0 & \boldsymbol{I} \\ \boldsymbol{I} & \boldsymbol{R} \end{bmatrix} \geq 0 \tag{21}$$

In the power systems, the set of initial states is composed of the unpredictable states of post-fault, so it is reasonable that X_0 is considered to be a hyper-ball in the following analysis without loss of generality, i.e., $\boldsymbol{P}_0 = \boldsymbol{I}$, then the (21) can be rewritten as

$$\begin{bmatrix} \gamma\boldsymbol{I} & \boldsymbol{I} \\ \boldsymbol{I} & \boldsymbol{R} \end{bmatrix} \geq 0 \tag{22}$$

Constraint (b) is equivalent to

$$\bar{u}_i^2 - \boldsymbol{g}_i(c\boldsymbol{P}^{-1})\boldsymbol{g}_i^{\mathrm{T}} \geq 0 \Leftrightarrow \bar{u}_i^2 - \boldsymbol{g}_i\boldsymbol{R}\boldsymbol{g}_i^{\mathrm{T}} \geq 0 \Leftrightarrow \begin{bmatrix} u_i^2 & \boldsymbol{g}_i \\ \boldsymbol{g}_i^{\mathrm{T}} & \boldsymbol{R}^{-1} \end{bmatrix} \geq 0 \Leftrightarrow \begin{bmatrix} 1 & 0 \\ 0 & \boldsymbol{R} \end{bmatrix} \begin{bmatrix} u_i^2 & \boldsymbol{g}_i \\ \boldsymbol{g}_i^{\mathrm{T}} & \boldsymbol{R}^{-1} \end{bmatrix} \begin{bmatrix} 1 & 0 \\ 0 & \boldsymbol{R} \end{bmatrix}^{\mathrm{T}} \geq 0 \Leftrightarrow \begin{bmatrix} u_i^2 & z_i \\ z_i^{\mathrm{T}} & \boldsymbol{R} \end{bmatrix} \geq 0, \quad i = 1, 2, \ldots, m \tag{23}$$

Constraint (c) can be transformed to

$$\boldsymbol{A}^{\mathrm{T}}\boldsymbol{P} + \boldsymbol{P}\boldsymbol{A} + \eta^{-1}\boldsymbol{P}\boldsymbol{E}\boldsymbol{E}^{\mathrm{T}}\boldsymbol{P} + \eta\alpha c^{-1}\boldsymbol{P} \leq 0 \Leftrightarrow \boldsymbol{R}\boldsymbol{A}^{\mathrm{T}} + \boldsymbol{A}\boldsymbol{R} + \eta_1\alpha\boldsymbol{E}\boldsymbol{E}^{\mathrm{T}} + \eta_1^{-1}\boldsymbol{R} \leq 0 \tag{24}$$

Since both η and η_1 are free variables, η_1 can be replaced by η for simplicity in (24), i.e., constraint (c) can be rewritten as

$$\boldsymbol{R}\boldsymbol{A}^{\mathrm{T}} + \boldsymbol{A}\boldsymbol{R} + \eta\alpha\boldsymbol{E}\boldsymbol{E}^{\mathrm{T}} + \eta^{-1}\boldsymbol{R} \leq 0 \tag{25}$$

4.2. Iterative algorithms for the optimization problem

From (21)–(25), problem (17) can be changed to the equivalent optimization problem as follows:

$$\begin{cases} (-\alpha^*, \gamma^*) = \min\limits_{R>0,\eta>0} (-\alpha, \gamma) \\ \text{s.t.} \quad \text{(a)} \quad \begin{bmatrix} \gamma\boldsymbol{I} & \boldsymbol{I} \\ \boldsymbol{I} & \boldsymbol{R} \end{bmatrix} \geq 0 \\ \qquad \text{(b)} \quad \begin{bmatrix} u_i^2 & z_i \\ z_i^{\mathrm{T}} & \boldsymbol{R} \end{bmatrix} \geq 0, \quad i = 1, 2, \ldots, m \\ \qquad \text{(c)} \quad \boldsymbol{R}\boldsymbol{A}^{\mathrm{T}} + \boldsymbol{A}\boldsymbol{R} + \eta\alpha\boldsymbol{E}\boldsymbol{E}^{\mathrm{T}} + \eta^{-1}\boldsymbol{R} \leq 0 \end{cases} \tag{26}$$

Lemma 3. *$(-\alpha^*,\gamma^*)$ is the POS of (26) if and only if (α^*,β^*) is that of (17).*

Proof. The conclusion is correct obviously. The proof is omitted. □

Lemma 3 shows that problem (17) can be converted to solve the POS of (26). But it is still very difficult to solve problem (26) due to the nonlinearities of constraint (c). Fortunately, if the parameter η is given, constraint (c) in (26) is also a LMI, which implies that certain iterative algorithm can used to handle it [17]. Namely, we can fix some variables to solve the others, and then reverse this process. Repeat these steps until a threshold is reached. Thus, problem (26) can be solved by the following algorithm:

IA-1 *((Iterative Algorithm 1 for problem (17)))*.

- Step 1: Initialize parameter η and fix it.
- Step 2: Solve the multi-objective LMI optimization problem (26) with fixed η.
- Step 3: Find a better value of η and go to step 2 until the convergence conditions are satisfied.

For the above algorithm IA-1, there are still two key problems difficult to handle. One is to solve the degenerative problem of (26) with fixed η; the other is to find a better value of η. In the following analysis, we give the algorithms and their theory foundations to handle the two problems.

For the first problem of IA-1, we note that when both η and α are fixed, problem (26) degenerates into a LMI optimization problem which can be solved easily. The degenerative model is

$$\gamma^* = \min_{\boldsymbol{R}>0}\gamma \tag{27}$$

s.t. constraints of optimization problem (26) with fixed α and η.

Similarly, when both γ and η are fixed, problem (26) degenerates into

$$-\alpha^* = \min_{\boldsymbol{R}>0} -\alpha \tag{28}$$

s.t. constraints of optimization problem (26) with fixed γ and η.

Hence, we can present the following two algorithms, say IA-A (Iterative Algorithm A) and IA-B (Iterative Algorithm B), to handle the first key problem in IA-1 mentioned above.

The main steps of IA-A are

- Step 1: Initialize variables η and α_0.
- Step 2: Calculate γ^* by optimization problem (27) with fixed η and α_0.
- Step 3: Calculate α^* by optimization problem (28) with fixed γ^* and η; consequently, obtain the $(-\alpha^*,\gamma^*)$, a POS of optimization problem (26) with the fixed η.

The main steps of IA-B are

- Step 1: Initialize variables η and γ_0.
- Step 2: Calculate α^* by optimization problem (28) with fixed η and γ_0.

- Step 3: Calculate γ^* by optimization problem (27) with fixed η and α^*; consequently, obtain the $(-\alpha^*,\gamma^*)$, a POS of optimization problem (26) with the fixed η.

To show that IA-A or IA-B does catch a POS of optimization problem (26) corresponding to a fixed η, we further introduce the following theorem, whose proof is given in Appendix A.

Theorem 3. *The result of IA-A (or IA-B), say $(-\alpha^*,\gamma^*)$, is one of the POS of problem (26) with fixed η.*

Proof. See Appendix A. □

As shown in Theorem 3, since IA-A (or IA-B) can obtain a POS, it can be concluded that if η in IA-A (or IA-B) is equal to that of the optimal solution of (26), the results derived by IA-A (or **B**) are the POS of (26). Thus, step 3 of IA-1 is reasonable.

For the second problem of IA-1, we use the golden section search (GSS) method [18] to search the better η in a pre-determined interval, such that the results of IA-A (or IA-B) increase along with the update of η. Therefore, based on the GSS method and IA-A (or IA-B), IA-1 can be implemented and the POS of problem (26) can be approximated by the following algorithms.

IA-2 *((Iterative Algorithm 2)).*

- Step 1: Initialize with $k=0$, $\alpha=\alpha_0$ and a reasonable interval $[c_0,d_0]$ for parameter η.
- Step 2: Set $\eta'_k=c_k+0.382l_k$ and $\eta''_k=c_k+0.618l_k$, where $l_k=d_k-c_k$.
- Step 3: Calculate the results, say $(-\alpha'^*_k, \gamma'^*_k)$ and $(-\alpha''^*_k, \gamma''^*_k)$, by IA-A with (η,α) being (η'_k, α_0) and (η''_k, α_0), respectively.
- Step 4: If $(-\alpha'^*_k, \gamma'^*_k) \le (-\alpha''^*_k, \gamma''^*_k)$, go to step 5; else go to step 6.
- Step 5: Set $d_{k+1}=\eta''_k$, $c_{k+1}=c_k$, $\eta''_{k+1}=c_{k+1}+0.618l_{k+1}$; calculate $(-\alpha''^*_{k+1}, \gamma''^*_{k+1})$ by IA-A with $(\eta,\alpha)=(\eta''_{k+1}, \alpha'^*_k)$; set $k=k+1$, $\alpha^*_k=\alpha''^*_k$, $\gamma^*_k=\gamma''^*_k$, and go to step 7.
- Step 6: Set $c_{k+1}=\eta'_k$, $d_{k+1}=d_k$, $\eta'_{k+1}=c_{k+1}+0.382l_{k+1}$; calculate $(-\alpha'^*_{k+1}, \gamma'^*_{k+1})$ by IA-A with $(\eta,\alpha)=(\eta'_{k+1}, \alpha''^*_k)$; set $k=k+1$, $\alpha^*_k=\alpha'^*_k$, $\gamma^*_k=\gamma'^*_k$, and go to step 7.
- Step 7: If $l_k>\varepsilon$, a pre-determined thresholding value, go to step 3; else go to step 8.
- Step 8: Set $\eta^*=0.5(c_k+d_k)$, $\alpha^*=\alpha^*_k$; calculate $(-\alpha^*,\gamma^*)$ by IA-A with $(\eta,\alpha)=(\eta^*,\alpha^*_k)$, then the $(-\alpha^*,\gamma^*)$, a POS of optimization problem (26), is founded.

From the fourth step to the seventh step in the above algorithm, we know that the better value of $(-\alpha,\gamma)$ is reserved as updating η. Hence, along with the convergence of η'_k and η''_k, the $(-\alpha^*_k, \gamma^*_k)$ increases, i.e., $(-\alpha^*_1, \gamma^*_1) \ge (-\alpha^*_2, \gamma^*_2) \ge \cdots \ge (-\alpha^*_k, \gamma^*_k) \ge \cdots$ is satisfied.

In the above algorithm, IA-1 is implemented by IA-2 using GSS and IA-A, however, based on the GSS method and the IA-B, IA-1 also can be implemented by the iterative algorithm as follows.

IA-3 *((Iterative Algorithm 3)).* Similar to those of IA-2, the steps of IA-3 are

- Step 1: Initialize with $k=0$, $\gamma=\gamma_0$ and a reasonable interval $[c_0,d_0]$ for parameter η.
- Step 2: Set $\eta'_k=c_k+0.382l_k$ and $\eta''_k=c_k+0.618l_k$, where $l_k=d_k-c_k$.
- Step 3: Calculate the results, say $(-\alpha'^*_k, \gamma'^*_k)$ and $(-\alpha''^*_k, \gamma''^*_k)$, by IA-B with (η,γ) being (η'_k, γ_0) and (η''_k, γ_0), respectively.
- Step 4: If $(-\alpha'^*_k, \gamma'^*_k) \le (-\alpha''^*_k, \gamma''^*_k)$, go to step 5; else go to step 6.
- Step 5: Set $d_{k+1}=\eta''_k$, $c_{k+1}=c_k$, $\eta''_{k+1}=c_{k+1}+0.618l_{k+1}$; calculate $(-\alpha''^*_{k+1}, \gamma''^*_{k+1})$ by IA-B with $(\eta,\gamma)=(\eta''_{k+1}, \gamma'^*_k)$; set $k=k+1$, $\gamma^*_k=\gamma''^*_k$, $\alpha^*_k=\alpha''^*_k$, and go to step 7.
- Step 6: Set $c_{k+1}=\eta'_k$, $d_{k+1}=d_k$, $\eta'_{k+1}=c_{k+1}+0.382l_{k+1}$; calculate $(-\alpha'^*_{k+1}, \gamma'^*_{k+1})$ by IA-B with $(\eta,\gamma)=(\eta'_{k+1}, \gamma''^*_k)$; Set $k=k+1$, $\gamma^*_k=\gamma'^*_k$, $\alpha^*_k=\alpha'^*_k$and go to step 7.
- Step 7: If $l_k>\varepsilon$, a pre-determined thresholding value, go to step 3; else go to step 8.
- Step 8: Set $\eta^*=0.5(c_k+d_k)$, $\gamma^*=\gamma^*_k$; calculate $(-\alpha^*,\gamma^*)$ by IA-B with $(\eta,\gamma)=(\eta^*,\alpha^*_k)$, then the $(-\alpha^*,\gamma^*)$, a POS of optimization problem (26), is founded.

From previous analysis, the sequences $(-\alpha^*_k, \gamma^*_k)(k=0,1,2,\ldots)$ derived by IA-2 or IA-3 can approximate the POS of (26) and satisfy $(-\alpha^*_1, \gamma^*_1) \ge (-\alpha^*_2, \gamma^*_2) \ge \cdots \ge (-\alpha^*_k, \gamma^*_k) \ge \cdots$. Thus, from the inverse transformation of (20) we can obtain the sequences (α^*_k, β^*_k) $(k=0,1,2,\ldots)$, corresponding to $(-\alpha^*_k, \gamma^*_k)(k=0,1,2,\ldots)$, which can approximate the POS of (17) and satisfy $(\alpha^*_0, \beta^*_0) \le (\alpha^*_1, \beta^*_1) \le (\alpha^*_1, \beta^*_1) \le \cdots \le (\alpha^*_k, \beta^*_k) \le \cdots$.

5. Saturated control performance analysis based on POS

5.1. Choice of the iterative algorithms and their initial parameters

A global optimal solution of the multi-objective optimization problem (17) may not exist [14]. Different initial values may lead to different POS and different algorithms also can yield different POS. Therefore, when applying the suggested method, one should make full use of engineering knowledge.

Since sequences (α_k,β_k) derived by IA-2 (or IA-3) satisfies $(\alpha^*_0, \beta^*_0) \le (\alpha^*_1, \beta^*_1) \le (\alpha^*_2, \beta^*_2) \le \cdots \le (\alpha^*_k, \beta^*_k) \le \cdots$, when the suggested method is applied to analyze the power systems with saturation nonlinearities and disturbance rejection, the following strategies can be implemented: if our concern is the stability region, for example, the estimated stability region Ω_0 needs to contain a ball with radium not less than $\bar{\beta}$, then we can select the IA-3 with $\gamma_0=\bar{\beta}^{-2}$. For this case, the path 1 of Fig. 1 shows the route of looking for POS by IA-3; otherwise if the issue is the disturbance rejection, for example, the maximum disturbance rejection needs be not less than $\bar{\alpha}$, then we can select the IA-2 with $\alpha_0=\bar{\alpha}$. For this case, the path 2 of Fig. 1 shows the route of looking for POS by IA-2.

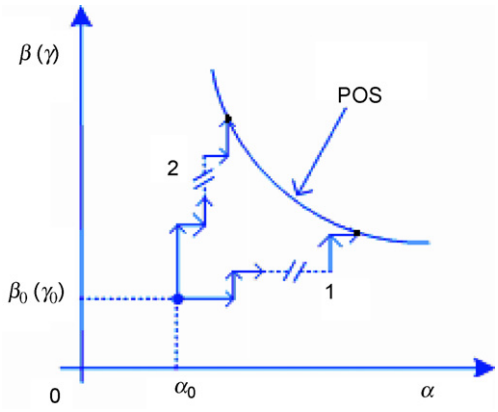

Fig. 1. Search route of IA-2 and IA-3.

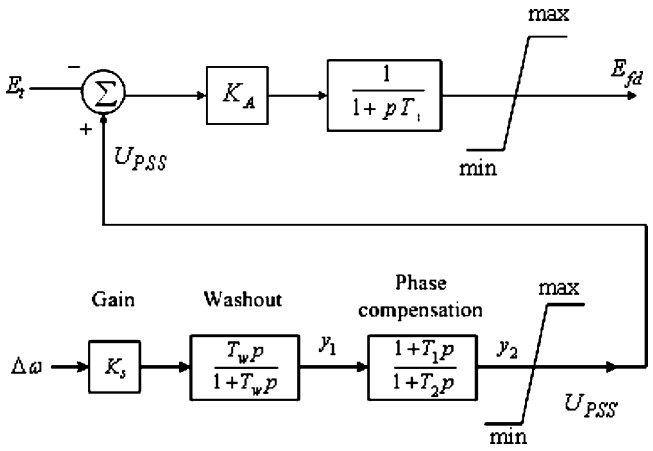

Fig. 2. Diagram of the excitation system and PSS Transfer Function.

5.2. Process of performance analysis of saturated controllers

As discussed above, problem (17) may not have a global optimal solution, so a reasonable goal is to find a practical POS, say (α^*,β^*). Based on the practical POS, the performance of the saturated controller, or the small-signal stability of power systems (4) can be analyzed by the following steps:

- Step 1: Is Assumption 1 satisfied or not? If yes, then continue; else, exit the algorithm.
- Step 2: Calculate the POS by IA-2 or IA-3. Select a practical result, say (α^*,β^*), to meet the engineering requirement.
- Step 3: Does the expected set of initial states and disturbance rejection set reside in their estimated regions? If yes, then the control law $\boldsymbol{u}=\boldsymbol{G}\boldsymbol{x}$ is effective; else, non-effective.

6. Simulations and results

In this section, we will apply the method (algorithms) derived previously to analyze the dynamic performance of a test power system with detailed saturated PSS controller models as an example.

6.1. The models of PSS with saturation nonlinearities and disturbance rejection

Suppose that the power system under study consists of N buses and n generators. We take the impedance model for loads, the model shown in Fig. 2 for AVR and PSS [1]. These models are also used in our recent paper [9], in which the disturbance rejection of PSS and AVR is not considered.

In this paper, we consider the saturated constraints are: (1) the output ($\Delta\boldsymbol{E}_{\mathrm{f}}$ in Fig. 2) of generator's excitation; (2) the output ($\boldsymbol{y}_2$ in Fig. 2) of the PSS control system. Namely, the constrained equations are

$$|\Delta\boldsymbol{E}_{\mathrm{f}i}| \le \Delta\bar{\boldsymbol{E}}_{\mathrm{f}i}, \ |\boldsymbol{y}_{2i}| \le \bar{\boldsymbol{y}}_{2i}, \quad i = 1, 2, \ldots, n \tag{29}$$

where $\Delta\bar{\boldsymbol{E}}_{\mathrm{f}i}$ is the upper saturation bound of $\Delta\boldsymbol{E}_{\mathrm{f}}$, the output of the ith generator's excitation; $\bar{\boldsymbol{y}}_{2i}$ is the upper saturation bound of $\boldsymbol{y}_2$, the output of the ith PSS control system.

Consider that the disturbance rejection results from stochastic disturbance imbed in the input signal of AVR and PSS, i.e., the $\Delta\boldsymbol{\delta}$ and $\Delta\boldsymbol{\omega}$ as input signal inputs contain noises, say $\boldsymbol{e}_1$ and $\boldsymbol{e}_2$, respectively.

Hence, if we let

$$\boldsymbol{y}=\left[\Delta\boldsymbol{\delta}^{\mathrm{T}}\ \Delta\boldsymbol{\omega}^{\mathrm{T}}\ \Delta\boldsymbol{E}_{\mathrm{q}}'^{\mathrm{T}}\ \middle|\ \Delta\boldsymbol{E}_{\mathrm{f}}^{\mathrm{T}}\ \middle|\ \boldsymbol{y}_1^{\mathrm{T}}\ \boldsymbol{y}_2^{\mathrm{T}}\right]^{\mathrm{T}},\ \bar{\boldsymbol{u}}=\left[\Delta\bar{\boldsymbol{E}}_{\mathrm{f}}^{\mathrm{T}}\quad \bar{\boldsymbol{y}}_2^{\mathrm{T}}\right]^{\mathrm{T}},\ \tilde{\boldsymbol{G}}=\left[\begin{array}{ccc|c|cc} \boldsymbol{0} & \boldsymbol{0} & \boldsymbol{0} & \boldsymbol{I} & \boldsymbol{0} & \boldsymbol{0} \\ \boldsymbol{0} & \boldsymbol{0} & \boldsymbol{0} & \boldsymbol{0} & \boldsymbol{0} & \boldsymbol{I} \end{array}\right] \tag{30}$$

then the closed-loop system after linearization can be expressed as

$$\dot{\boldsymbol{y}} = \tilde{\boldsymbol{A}}\boldsymbol{y} + \tilde{\boldsymbol{E}}w \tag{31}$$

$$-\bar{\boldsymbol{u}} \le \tilde{\boldsymbol{G}}\boldsymbol{y} \le \bar{\boldsymbol{u}} \tag{32}$$

For more information about the variable in (30)–(32), readers are referred to Refs. [1,9].

In system (31)–(32), matrix $\tilde{A}$ has a zero eigenvalue and specially two zero eigenvalues with uniform damping coefficients [1]. For this case, a reference machine, say the nth generator, is chosen to obtain the equivalent reduced-order model, which satisfies Assumption 1. This process can be easily done for the systems with uniform damping coefficients via the following transformation [9]:

$$\boldsymbol{A} = \boldsymbol{S}\tilde{\boldsymbol{A}}\cdot\mathrm{pinv}(\boldsymbol{S}), \quad \boldsymbol{G} = \tilde{\boldsymbol{G}}\cdot\mathrm{pinv}(\boldsymbol{S});$$
$$\boldsymbol{x} = \boldsymbol{S}\boldsymbol{y}, \quad \boldsymbol{E} = \tilde{\boldsymbol{E}}\cdot\mathrm{pinv}(\boldsymbol{S}) \tag{33}$$

where $\boldsymbol{S}=\mathrm{diag}\{\boldsymbol{s}_1,\boldsymbol{s}_1,\boldsymbol{s}_2\}$, $\boldsymbol{s}_1=[\boldsymbol{I}_{(ng-1)\times(ng-1)}|\boldsymbol{e}]$, $\boldsymbol{s}_2=\boldsymbol{I}_{4ng\times 4ng}$, $\boldsymbol{e}=-[\overbrace{1,1,\cdots 1}^{ng-1}]^{\mathrm{T}}$ and symbol pinv(·) denotes generalized inverse function [18].

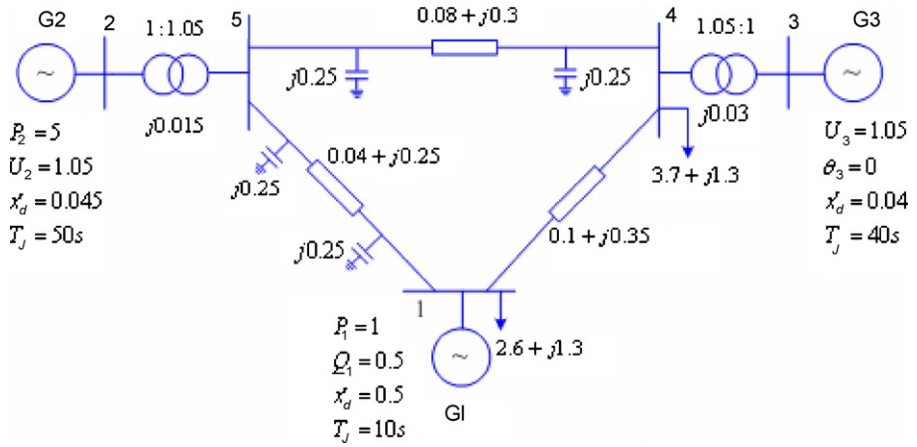

Fig. 3. Diagram of the three-bus system.

Thus, from (31)–(33), the equivalent model of (31)–(32) degenerates into

$$\dot{\boldsymbol{x}} = \boldsymbol{A}\boldsymbol{x} + \boldsymbol{E}\boldsymbol{w} \tag{34}$$

$$-\bar{\boldsymbol{u}} \le \boldsymbol{G}\boldsymbol{x} \le \bar{\boldsymbol{u}} \tag{35}$$

Model (34)–(35) satisfies Assumption 1. We will use them to analyze the effectiveness of PSS control system and the small-signal stability of power systems in the following section.

Remark 2.

1. It should be noted that the method we suggested is not restricted to the dynamic models of PSS and AVR as what we have selected. In fact, as long as the linearization model of a power system can be expressed as (31)–(32) or (34)–(35), then the method works.
2. In power systems, we usually can directly obtain the dynamic models such as system (31) or (34) for small-signal stability analysis from a software package, so we only need to set up the saturation constraint equations when applying the suggested method. Hence, we extended model (4) to model (16), such that it is very easy to apply the method to a large power system with more complex models, such as various models of PSS and dynamic models of loads, etc.

6.2. Results

To illustrate the methods (algorithms) discussed previously, a test system with three generator and five buses is used. The diagram of this test system is shown in Fig. 3. The data of this test system are shown in Appendix B, including the data of PSS and AVR.

The parameters are initialized as follows: the range for η is [8,40]; our concern here is the stability region, i.e., the stability region needs contain a ball with radium more than 0.05, so $\beta_0 = 5\%$ is taken. Using the methods (algorithms) addressed previously, we first calculate the stability region and the corresponding POS for the power system stability analysis, i.e., to decide the maximum magnitude of disturbance rejection that the power system can withstand and meanwhile to decide the maximum excursion of the initial states of the system based on these results. Second, we want to analyze the impact of the saturation bound in the power system on the stability regions and the POS. As such, we can obtain some conclusions about the impact of a saturation constraint such as the constraint of a generator's exciter on the power system stability to some extent. Thus, we perform the following simulations.

6.2.1. Stability regions and the POS

By IA-3, the (0.053, 0.072), one of the POS, is derived, and the corresponding optimal solution of η is 21.017, i.e., $\max(\alpha,\beta) = (0.053, 0.072)$ and $\eta^* = 21.017$. For this POS, from previous analysis, we can draw the conclusion that, if the initial states reside in a ball with radium of $\beta^* = 0.072$ and the disturbance rejection resides in a ball with radium of $\sqrt{\alpha^*} = \sqrt{0.053} = 0.230$, then the PSS control system can stabilize this system, which can also be checked by the results of time domain simulations as shown in Fig. 4, here the magnitude (2-norm) of initial state and disturbance rejection are 0.06 and 0.21, respec-

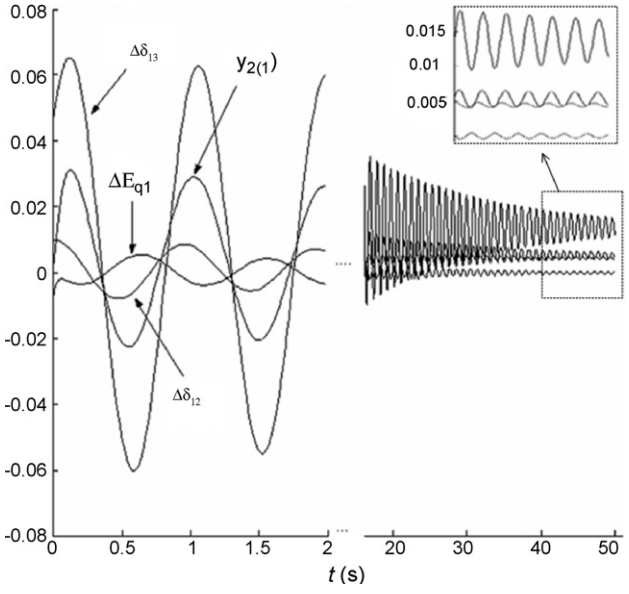

Fig. 4. Results of the time domain by simulations.

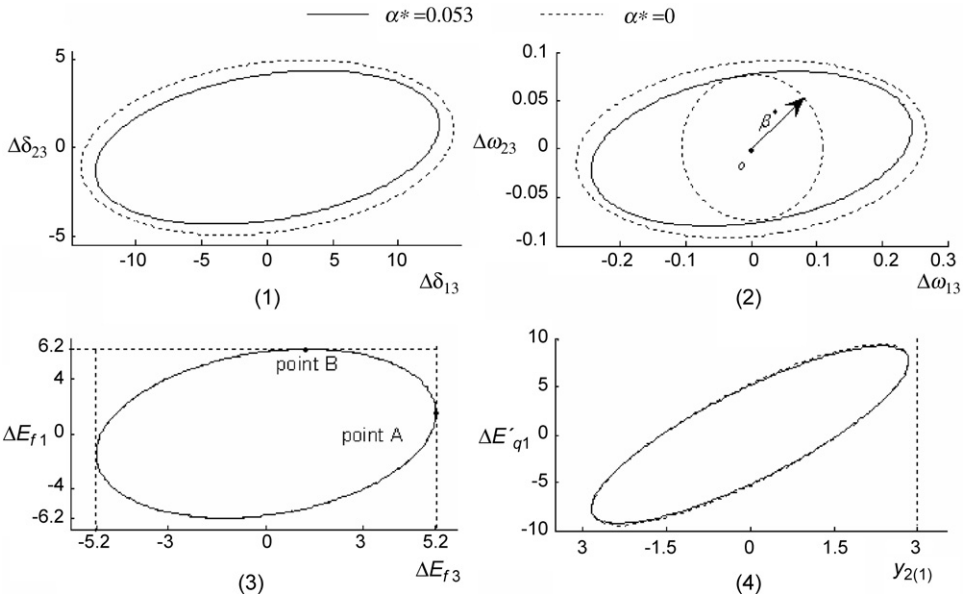

Fig. 5. Projections of the attractive regions.

tively. However, if IA-2 with $\alpha_0 = 0$ is applied instead of IA-3, (0.0, 0.081), another POS, can be obtained. This is consistent with the fact that the POS are not unique. In fact, (0.0, 0.081) is the optimal result of paper [9], so the method in this paper is the extension of [9] when the disturbance rejection is considered. Moreover, the projections of the estimated stability regions corresponding to these two POS are depicted by Fig. 5, where the real ellipses denote the projections of the stability region corresponding to (0.053, 0.072) and the dash ellipses denote those corresponding to (0.0, 0.081).

Next, we analyze the relationship between the stability region (the maximum set of initial states) and the maximum endurable disturbance rejection for the system. In Fig. 5, the maximum set of initial states (a ball in our simulation as mentioned previously) in the estimated stability region of nominal system (no disturbance rejection) is larger than that of the system with disturbance rejection. In fact, the phenomena are common, since the energy of controller is finite due to saturation nonlinearities, when the energy of disturbance rejection increases, the energy of initial states must decrease so that the controller can guarantee the system stability. Thus, disturbance rejection will minish estimated stability region, and the more the disturbance rejection (α^*) is, the smaller the maximum ball (β^*) contained by estimated stability region is. This conclusion also can be illustrated by curve (b) of Fig. 6, where curve (b) is the POS of problem (17) and it also validates Theorem 2, i.e., β^* decreases when α^* increases.

To show that the GSS method we constructed for IA-1 works well, we compare the results of IA-A in which we did not optimize η and those of IA-2 in which we have optimized η. It can be imaged that the results of POS are more conservative than that uses GSS method. In fact, the GSS method works well in this optimization problem, this conclusion can be illustrated by Fig. 6, where curve (a) denotes the POS by IA-A with fixed parameter ($\eta = 15$), and curve (b) denotes the POS by IA-2 which has used the GSS method. It is evident that the results of IA-A are more conservative than those of IA-2, this is because the results of IA-A are not the POS of optimization problem (17) but those of (27).

6.2.2. *Impacts of saturation bound on the pos and the stability regions*

Now let us get back to Fig. 5 to show the relaxation of some saturation constraint has evident impact on the active constraints [9] in the optimization problem (17). In the third sub-figure which depicts the projection of stability region on coordinate $\Delta E_{f3} - \Delta E_{f1}$, we note that the excitation constraints of generators 1 and 3 are tangent with stability region at point B and point A, respectively. Hence, the excitation saturation constraints of generators 1 and 3 are active constraints, i.e., the inequality constraint (b) in the expression (23) become equality constraints when the index i is equal to 1 or 3. However, from the fourth sub-figure, the saturation constraint of the third PSS is not tangent with the stability region, so it is not an active constraint. But

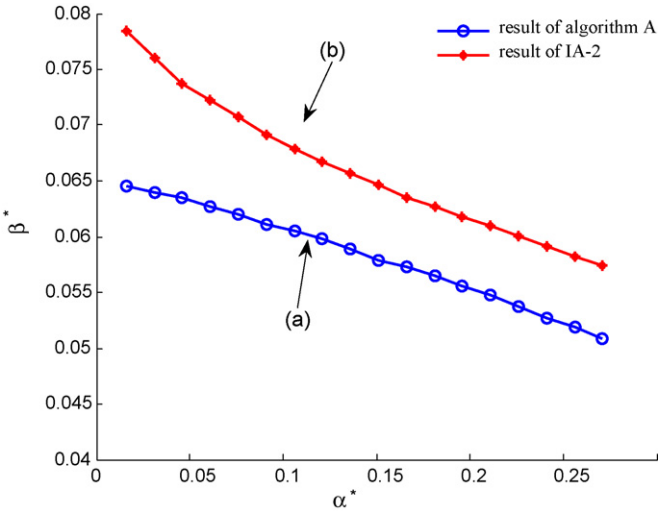

Fig. 6. POS of the test system by IA-A and IA-2.

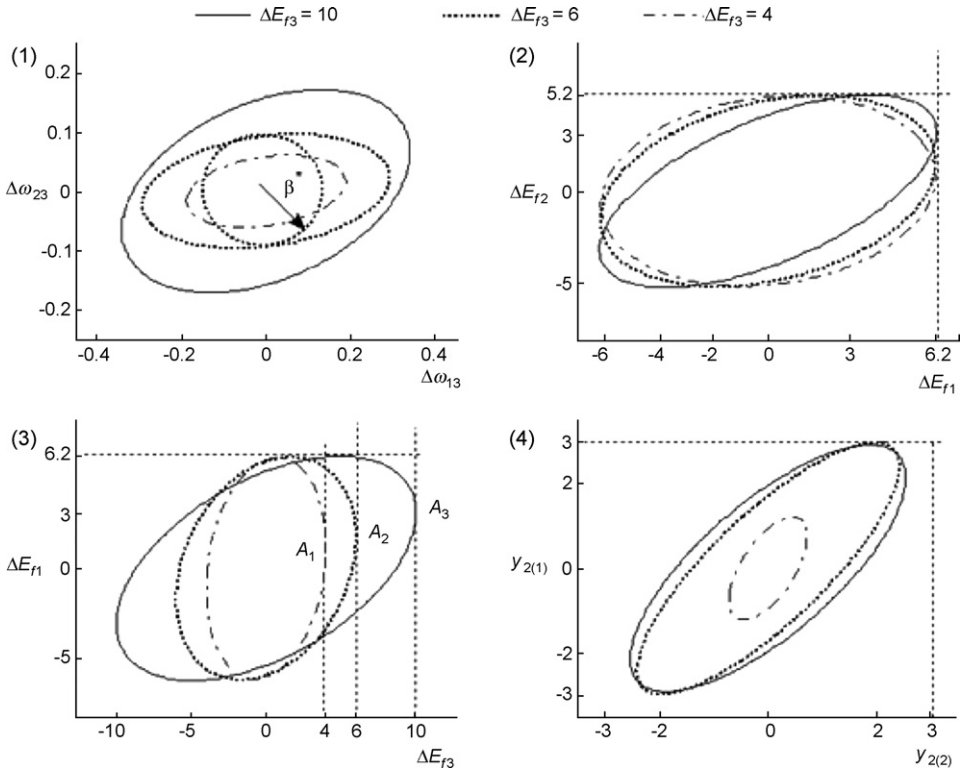

Fig. 7. Relationship between stability region and saturation bound.

when the saturation bound $\Delta\bar{E}_{f3}$ is changed and other parameters are fixed, i.e., only the saturation bound of generator 3 is changed, the stability region changes rapidly. Fig. 7 shows the projections of the corresponding estimated stability regions, where $\Delta\bar{E}_{f3}$ is 4.0, 6.0, and 10.0, respectively. In Fig. 7, we can find that when $\Delta\bar{E}_{f3}$ increases to 6.0, the saturation bound of the PSS output of generator 1, $\bar{y}_{2(1)} = 3$, is also tangent with the estimated stability region on coordinates $y_{2(1)} - y_{2(2)}$. Namely, the active constraints are changed, i.e., the saturation constraints of exciters are still active, but the PSS output of generator 1 becomes the active constraint.

The change of saturation bound $\Delta\bar{E}_{f3}$ can also have impact on the POS of problem (17) and on η^*. Fig. 8 shows the relationship between the POS and the upper bound $\Delta\bar{E}_{f3}$ and Fig. 9 shows the relationship between α^* and η^*. In Fig. 8, it can be observed that the curves of POS with bigger $\Delta\bar{E}_{f3}$ are above the curves with smaller $\Delta\bar{E}_{f3}$, so the relaxation of the saturation constraints can lead to the increase of POS monotonously. However, from Fig. 9, we can find that for the same α^*, the curve with $\Delta\bar{E}_{f3} = 5.2$ is not above the curve with $\Delta\bar{E}_{f3} = 7.2$ but is above that with $\Delta\bar{E}_{f3} = 10$, thus, the change of η^* has no monotonous property as the relaxation of the saturation constraints. Nevertheless, the η^* is decreasing monotonously with the increase of α^* from Theorem 2 or from Fig. 6. This important observation can help us select the range for η in the initialization step in the iterative algorithms such as IA-2 and IA-3.

When $\Delta\bar{E}_{f3}$ is small enough, the active constraints are only the saturation of ΔE_{f3} and the POS is only determined by this constraints. But when bound $\Delta\bar{E}_{f3}$ is big enough, the POS is not only determined by the saturation of the exciter's outputs, but also determined by the saturation of PSS's outputs. This conclusion can be easily confirmed by Fig. 8, where, the change of $\Delta\bar{E}_{f3}$ has an apparent impact on the POS when $\Delta\bar{E}_{f3}$ is smaller than 10. When $\Delta\bar{E}_{f3}$ is larger than 10, along with the change of $\Delta\bar{E}_{f3}$ from 10 to 12, the POS remain nearly constant and so does the corresponding optimal parameter (η^*). In other words, in power systems the saturation bounds have large impact on the performance of controllers and on the small-signal stability. Moreover, it is only when the saturation bound of a exciter's

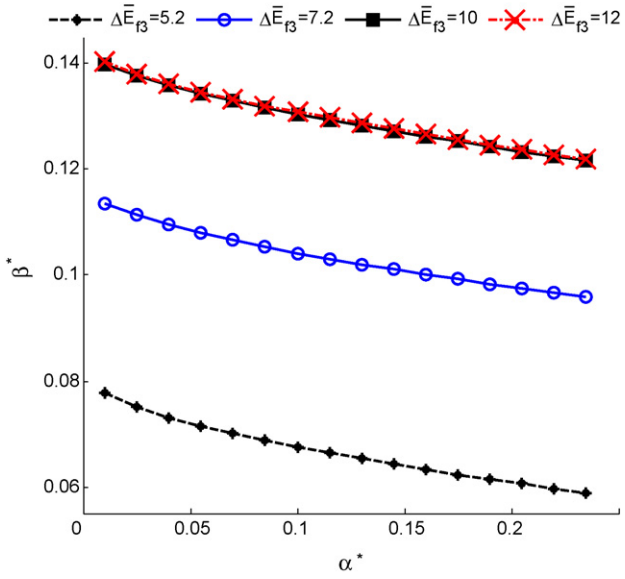

Fig. 8. Relationship between POS and the saturation bound.

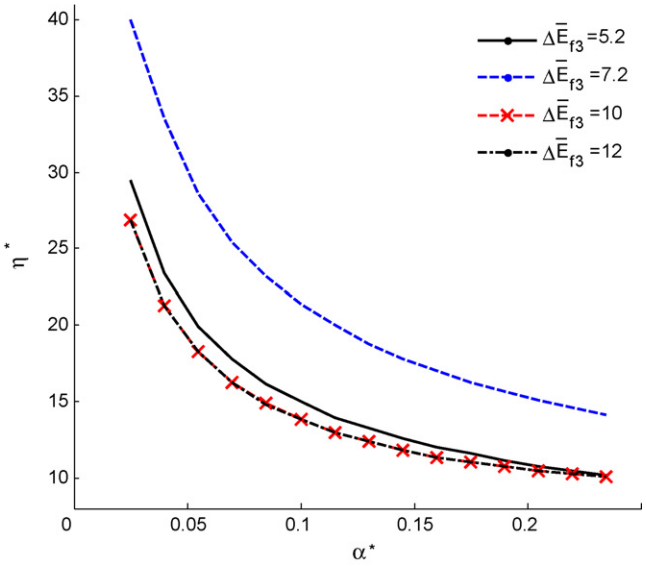

Fig. 9. Relationship between η^* and the saturation bounds.

output is small enough that turning the exciter's output bound is useful to improve the power system small-signal stability. Otherwise, tuning of the saturation bounds need be considered synthetically.

7. Conclusion

In this paper, we provide an analytical method to analyze the impact of saturation nonlinearities and disturbance rejections on the small-signal stability of power systems. As an application, we choose to study the performance of a PSS controller with nonlinearity saturation and disturbance rejections. To improve the accuracy of the results, a multi-objective optimization model based on LMI is introduced and algorithms for solving the problem are developed. The properties of the algorithms are proved also. The simulation results of a test power system demonstrate that the method is effective.

Acknowledgements

This research is jointly supported by the Natural Science Foundation (Project 50595411) of China and Department of Education of China under New Century Outstanding Investigator program.

Appendix A

To describe the following analysis clearly, we introduce some abbreviations as follows. Let $\mathfrak{Q}$ denote the feasible region of optimization problem (26), i.e., for every $(\boldsymbol{R}, \gamma, \alpha, \eta) \in \mathfrak{Q}$, $(\boldsymbol{R},\gamma,\alpha,\eta)$ is a solution satisfying the constraints of (26); Let $\mathfrak{Q}_\eta$, $\mathfrak{Q}_{\eta,\alpha}$ and $\mathfrak{Q}_{\eta,\gamma}$ denote the $\mathfrak{Q}$ with fixed η, (η,α) and (η,β), respectively. Clearly, from our previous analysis, we know that $\mathfrak{Q}_{\eta,\alpha}$ is the feasible region of (27) with fixed (η,α); and $\mathfrak{Q}_{\eta,\gamma}$ is the feasible region of (28) with fixed (η,γ).

First of all, to prove the theorem we introduce the following Lemma.

Lemma 4. *In IA-A (or IA-B), $\alpha_0 \le \alpha^*$ (or $\gamma_0 \ge \gamma^*$). Here, α_0 (or γ_0) is the initial value of α (or γ); α^* (or γ^*) is the result of IA-A (or IA-B).*

Proof. We only prove the conclusion for IA-A since the proof for IA-B is similar.

In the second step of IA-A, γ^* is the optimal value of optimization problem (27) with fixed η and α_0, and we let $\boldsymbol{R}_1$ denote the optimal value corresponding to $\boldsymbol{R}$, thus $(\boldsymbol{R}_1,\gamma^*,\alpha_0,\eta)$ satisfies the constraints of (26), i.e., $(\boldsymbol{R}_1, \gamma^*, \alpha_0, \eta) \in \mathfrak{Q}$, which implies $(\boldsymbol{R}_1, \alpha_0) \in \mathfrak{Q}_{\eta,\gamma^*}$ from the definition of $\mathfrak{Q}_{\eta,\gamma}$. Similarly, in the third step of IA-A, α^* is the optimal value of problem (28) with fixed η and γ^*, and we let $\boldsymbol{R}_2$ denote the optimal value of $\boldsymbol{R}$, so $(\boldsymbol{R}_2,\gamma^*,\alpha^*,\eta)$ satisfies the constraints of (26), i.e., $(\boldsymbol{R}_2, \gamma^*, \alpha^*, \eta) \in \mathfrak{Q}$, which implies $(\boldsymbol{R}_2, \alpha^*) \in \mathfrak{Q}_{\eta,\gamma^*}$ from the definition of $\mathfrak{Q}_{\eta,\gamma}$. Hence, both $(\boldsymbol{R}_1, \alpha_0) \in \mathfrak{Q}_{\eta,\gamma^*}$ and $(\boldsymbol{R}_2, \alpha^*) \in \mathfrak{Q}_{\eta,\gamma^*}$ are satisfied. Since α^* is the maximum value of problem (27) with the fixed η and γ^*, i.e., α^* is the maximum value among all of variables satisfying $(\boldsymbol{R}, \alpha) \in \mathfrak{Q}_{\eta,\gamma^*}$. Consequently, $\alpha_0 \le \alpha^*$. □

Now we can prove Theorem 3 on the basis of Lemma 4.

Theorem 3. *The result of IA-A (or IA-B), say $(-\alpha^*,\gamma^*)$, is one of the POS of problem (26) with fixed η.*

Proof. Since the proof for IA-B is alike, we only prove the conclusion for IA-A, i.e., $(-\alpha^*,\gamma^*)$ is a POS of (26) with fixed η. To show this conclusion, we use a contradiction argument.

Suppose that $(-\alpha^*,\gamma^*)$ is not a POS of (26) with fixed η. Thus, from the definition of POS, there exists a $(\boldsymbol{R}', \gamma', \alpha') \in \mathfrak{Q}_\eta$ satisfying $(-\alpha',\gamma') < (-\alpha^*,\gamma^*)$, which implies that $\alpha' \ge \alpha^*$ and $\gamma' \le \gamma^*$. From Lemma 4 $\alpha^* \ge \alpha_0$ holds, and consider again that both $\alpha' \ge \alpha^*$ and $\gamma' \le \gamma^*$ hold, so observing the constraints of (26), we easily get that $(\boldsymbol{R}', \gamma', \alpha') \in \mathfrak{Q}_\eta$ implies that both $(\boldsymbol{R}', \gamma', \alpha_0) \in \mathfrak{Q}_\eta$ and $(\boldsymbol{R}', \gamma*, \alpha') \in \mathfrak{Q}_\eta$ hold. Furthermore, the following expressions are satisfied from the definition of $\mathfrak{Q}_{\eta,\alpha_0}$ and $\mathfrak{Q}_{\eta,\gamma^*}$:

$$(\boldsymbol{R}', \gamma') \in \mathfrak{Q}_{\eta,\alpha_0}, \quad (\boldsymbol{R}', \alpha') \in \mathfrak{Q}_{\eta,\gamma^*} \tag{36}$$

We know that γ^* is the minimum value among the variables satisfying $(\boldsymbol{R}, \gamma) \in \mathfrak{Q}_{\eta,\alpha_0}$ from the second step of IA-A, so $\gamma^* \le \gamma'$ is satisfied from $(\boldsymbol{R}', \gamma') \in \mathfrak{Q}_{\eta,\alpha_0}$ in (36). Consequently, from $\gamma' \le \gamma^*$ and $\gamma^* \le \gamma'$, we get $\gamma' = \gamma^*$. Similarly, we know that α^* is the maximum value among the variables satisfying $(\boldsymbol{R}, \alpha) \in \mathfrak{Q}_{\eta,\gamma^*}$ from the third step of IA-A, so $\alpha' \le \alpha^*$ holds from $(\boldsymbol{R}', \alpha') \in \mathfrak{Q}_{\eta,\gamma^*}$ in (36). Consequently, from $\alpha' \le \alpha^*$ and $\alpha' \ge \alpha^*$, we get $\alpha' = \alpha^*$. Therefore, both $\gamma' = \gamma^*$ and $\alpha' = \alpha^*$ holds. It is contradictory with assumption $(-\alpha',\gamma') < (-\alpha^*,\gamma^*)$. Thus, the conclusion is proved. □

Appendix B

In this appendix, we give the parameters of the generators, PSS and exciter's controllers in Fig. 3.

Generator 1: $P_1 = 1$, $Q_1 = 0.5$, $x'_d = 0.5$, $H = 5s$, $D = 0.005$, $T'_{do} = 5.35$; $K_A = 6$, $T_A = 0.02(s)$; $K_s = 1.0$, $T_w = 5.0(s)$, $T_1 = 0.35(s)$, $T_2 = 0.03(s)$; $\Delta\bar{E}_{f1} = 6.2$, $\bar{y}_2 = 3.0$.

Generator 2: $P_2 = 5$, $U_2 = 1.05$, $x'_d = 0.045$, $H = 25s$, $D = 0.025$, $T'_{do} = 5.35$; $K_A = 10$, $T_A = 0.02(s)$; $K_s = 1.0$, $T_w = 8.3(s)$, $T_1 = 0.35(s)$, $T_2 = 0.03(s)$; $\Delta\bar{E}_{f1} = 5.2$, $\bar{y}_2 = 3.0$.

Generator 3: $\theta_3 = 0$, $U_3 = 1.05$, $D = 0.020$, $H = 20s$, $x'_d = 0.04$, $T'_{do} = 3.76$; $K_A = 17.5$, $T_A = 0.02(s)$; $K_s = 1.0$, $T_w = 8.0(s)$, $T_1 = 0.45(s)$, $T_2 = 0.05(s)$; $\Delta\bar{E}_{f1} = 5.2$, $\bar{y}_2 = 3.0$.

References

[1] P. Kundur, Power System Stability and Control, McGraw-Hill, New York, 1994.

[2] P. Zhang, A.H. Coonick, Coordinated synthesis of PSS parameters in multi-machine power systems using the method of inequalities applied to genetic algorithms, IEEE Trans. Power Syst. 15 (2000) 811–816.

[3] P.S. Rao, E.S. Boje, A quantitative design approach to PSS tuning, Electric Power Syst. Res. 73 (2005) 249–256.

[4] W. Qiu, V. Vittal, M. Khammash, Decentralized power system stabilizer design. Using linear parameter varying approach, IEEE Trans. Power Syst. 19 (2004) 1951–1960.

[5] C.T. Tse, K.W. Wang, C.Y. Chung, K.M. Tsang, Robust PSS design by probabilistic eigenvalue sensitivity analysis, Electric Power Syst. Res. 59 (2001) 47–54.

[6] T. Hu, Z. Lin, Control Systems with Actuator Saturation: Analysis and Design, Birkhauser, Boston, 2001.

[7] R. Escarela-Perez, T. Niewierowicz, E. Campero-Littlewood, A study of the variation of synchronous machine parameters due to saturation: a numerical approach, Electric Power Syst. Res. 72 (2004) 1–11.

[8] M.L. Crow, J. Ayyagari, The effect of excitation limits on voltage stability, IEEE Trans. Circuits Syst. I: Fundam. Theory Appl. 42 (1995) 1022–1026.

[9] H. Xin, D. Gan, T.S. Chung, J.J. Qiu, A method for evaluating the performance of PSS with saturated input, Electric Power Syst. Res. 77 (2007) 1284–1291.

[10] H.K. Khalil, Nonlinear Systems, 2nd ed., Prentice-Hall, New Jersey, 1996.

[11] Z. Qu, Robust Control of Nonlinear Uncertain Systems, Wiley, New York, 1998.

[12] H. Hindi, S. Boyd, Analysis of linear systems with saturation using convex optimization, in: Proceedings of the 37th IEEE Conference on Decision & Control, Florida, 1998, pp. 903–908.

[13] T. Hu, Z. Lin, B.M. Chen, An analysis and design method for linear systems subject to actuator saturation and disturbance, Automatica 38 (2002) 351–359.

[14] K. Deb, Multi-Objective Optimization Using Evolutionary Algorithms, John Wiley & Sons Ltd., England, 2001.

[15] D. Gan, Z. Qu, H. Cai, Multi-machine system excitation control via theories of feedback linearization control and nonlinear robust control, Int. J. Syst. Sci. 31 (2000) 519–527.

[16] D. Gan, R.J. Thomas, R.D. Zimmerman, Stability-constrained optimal power flow, IEEE Trans. Power Syst. 5 (2000) 535–540.

[17] Y. Cao, Z. Lin, D.G. Ward, An anti-windup approach to enlarging domain of attraction for linear systems subject to actuator saturation, IEEE Trans. Autom. Contr. 47 (2002) 140–145.

[18] M.S. Bazaraa, H.D. Sherali, C.M. Shetty, Nonlinear Programming—Theory and Algorithms, 2nd ed., John Wiley & Sons, 1993.

Huanhai Xin is a Ph.D. candidate in the College of Electrical Engineering, Zhejiang University. His research interests include power system stability analysis and control.

Deqiang Gan has been with the faculty of Zhejiang University since 2002. Deqiang visited the University of Hong Kong in 2004. He was a Senior Analyst in ISO New England, Inc. from 1998 to 2002. Deqiang held research positions in Ibraki University, University of Central Florida, and Cornell University from 1994 to 1998. He received a Ph.D. in Electrical Engineering from Xian Jiaotong University, China, in 1994. Deqiang is an editor of European Transactions on Electrical Power. His research interests are in the applications of nonlinear system and game theory to power systems.

Zhihua Qu received his Ph.D. from School of Electrical Engineering, Georgia Institute of Technology, Atlanta, GA in June 1990. Since then, he has been with Department of Electrical and Computer Engineering, University of Central Florida and currently holds the rank of Professor. His research interests are control and system theory with application to power systems and robotics.

Jiaju Qiu is a professor of Electrical Engineering in Zhejiang University. He received a Ph.D. in 1988 from the same university where he teaches and conducts research in the general area of power engineering. Professor Qiu has over 10 years of industry experiences; he visited the University of Strathclyde and Cornell University in 1993, 1994, respectively.